Journal of Alloys and Compounds 702 (2017) 372–380

Contents lists available at ScienceDirect

Journal of Alloys and Compounds

journal homepage: http://www.elsevier.com/locate/jalcom

# Ti-doped $Fe_{1-x}Ti_xF_3 \cdot 0.33H_2O$/C nanocomposite as an ultrahigh rate capability cathode materials of lithium ion batteries

Shuangying Wei, Xianyou Wang*, Ruizhi Yu, Rui Zhang, Min Liu, Zhenhua Yang, Hai Hu

*National Base for International Science & Technology Cooperation, National Local Joint Engineering Laboratory for Key Materials of New Energy Storage Battery, Hunan Province Key Laboratory of Electrochemical Energy Storage and Conversion, School of Chemistry, Xiangtan University, Hunan, Xiangtan 411105, China*

ARTICLE INFO

*Article history:*
Received 20 November 2016
Received in revised form
19 January 2017
Accepted 21 January 2017
Available online 25 January 2017

*Keywords:*
Lithium ion batteries
Ti-doping
Iron fluoride
Cathode material
Electrochemical performance

ABSTRACT

The conductivity problem of $FeF_3 \cdot 0.33H_2O$ is the main constraint on development and application of this next-generation cathode material for lithium/sodium ion batteries. It has been found in our previous theoretical calculation that Ti-doping can dramatically improve the conductivity $FeF_3 \cdot 0.33H_2O$, and thus improving its electrochemical performance. Herein, Ti-doped $Fe_{1-x}Ti_xF_3 \cdot 0.33H_2O$ (x = 0, 0.06, 0.08, 0.10) compounds have been successfully synthesized via a liquid-phase method. Subsequently, a ball milling process with acetylene black (AB) has been used to form $Fe_{1-x}Ti_xF_3 \cdot 0.33H_2O$/C ($x$ = 0, 0.06, 0.08, 0.10) nanocomposite. The chemical composition and elemental distribution of the Ti-doped $FeF_3 \cdot 0.33H_2O$ samples were investigated by X-ray diffraction (XRD) and energy-dispersive X-ray spectroscopy (EDXs). The results show that Ti can effectively dope into the samples, and replace partially $Fe^{3+}$ ions in the $FeF_3 \cdot 0.33H_2O$ crystal. Especially the $Fe_{0.92}Ti_{0.08}F_3 \cdot 0.33H_2O$/C nanocomposite achieves an initial capacity of 460.15 mAh $g^{-1}$ and retains a discharge capacity of 294.86 mAh $g^{-1}$ after 40 cycles in the voltage range of 1.5–4.5 V. Besides, the as-prepared material shows excellent rate capability, it can deliver a discharge capacity of 146.06 mAh $g^{-1}$ even at 2 C.



## 1. Introduction

In order to improve lithium ion batteries (LIBs) performance with satisfactory power and energy density, masses of new cathode materials have been explored [1]. Currently, the conversion reactions between alkali metals and electrode materials, which do not primarily rely on the size of alkali cations, seems to be a promising strategy to achieve high capacity of electrodes materials for LIBs. Among them, multi-electron materials, especially transition metal fluorides, have attracted substantial interest because all oxidation states of the active material can be utilized and high specific capacities are supplied, which is quite different from cathode materials based on intercalation mechanism [2–4]. Since the iron trifluoride ($FeF_3$) was firstly reported for LIBs by Arais's, it has attracted extensively attention due to its high voltage plateau, high theoretical specific capacity (712 mAh $g^{-1}$ for 3 $e^-$ transfer), low cost, and environmental friendliness [1,5]. In addition, the strong Fe-F ionic bonds in the $FeF_3$ sample is expected to provide a high discharge capacity and high redox voltage when applied in cathode materials for LIBs [6,7]. However, the high ionicity is the main problem restricting its practical application of cathode material, which induces a large bandgap of Fe-F, leading to a poor electronic conductivity, thus making the actual specific capacity is significantly lower than the theoretical value [8,9].

To further improve the electronic conductivity of the iron fluoride, various endeavors have been carried out, such as decreasing size of particles and forming composite with conductive materials (graphite, carbon black, active carbon, etc). $FeF_3$ and carbon material were mixed followed by ball-milling to form carbon-metal-fluoride nanocomposites (CMFNCs), which deliveries a reversible specific capacity of 216 mAh·$g^{-1}$ in a voltage range of 2.8–3.5 V and a reversible specific capacity of 447 mAh $g^{-1}$ between 1.5 and 2.5 V at a low current density of 7.58 mA $g^{-1}$ [10]. The CMFNCs shows higher specific capacity, but the cyclic property of these composites is worse. Li et al. prepared the $FeF_3$/GO nanocomposites via chemical synthesis route and obtained a high reversible specific capacity of about 700 mAh $g^{-1}$ between 1.0 and 4.5 V at 100 mA $g^{-1}$, but a short cycling test with only 10 cycles was displayed [11].

Constructing novel nanostructures is an alternative approach to

* Corresponding author.
*E-mail address:* wxianyou@yahoo.com (X. Wang).

http://dx.doi.org/10.1016/j.jallcom.2017.01.240
0925-8388/

improve the electrochemical property of the iron fluoride. For example, Li et al. [12–17] developed a series of iron fluoride with open framework. Among them, nanoscale $FeF_3{\cdot}0.33H_2O$ has attracted tremendous attention due to its unique tunnel structure [15–17]. The tunnel structure is beneficial to facilitate electrolyte penetration and $Li^+$ transport. By hybridizing $FeF_3$ with a conductive additive phase (such as SWNTs, 3DOM, CNHs, rGO, ordered mesoporous carbon and carbon nanohorns) can provide a facile electron pathway. Zhang et al. synthesized three-dimensionally ordered macroporous (3DOM) $FeF_3$/poly (3,4-ethylenedioxythiophene) (PEDOT) composite through in situ polymerization method. It has been found that the composite can deliver 210 mAh $g^{-1}$ at 20 mA $g^{-1}$ and a good rate capability of 120 mAh $g^{-1}$ at 1 A $g^{-1}$ in a voltage range of 2.0–4.5 V [18]. Li and his coworkers prepared SWNTs/$FeF_3{\cdot}0.33H_2O$ in the $BmimBF_4$ medium via a precipitation method, which exhibit remarkable rate performance (220 mAh $g^{-1}$ at 0.1 C and 80 mAh $g^{-1}$ at 10 C, 1 C = 237 mA $g^{-1}$) and better cycling performance (143 mAh $g^{-1}$ at 0.1 C after 30 cycles) between 1.7 and 4.5 V [17]. Namely, the introduction of conductive polymer or carbon can greatly improve the electrochemical performance of iron fluoride. However, it is not worthwhile for the aspect of cost since $BmimBF_4$ ionic liquid and SWNTs are very expensive. Additionally, when relating to polymer, it will inevitably involve the harmful organic solvents usage, cumbersome synthesis process and post-processing. Our group has successfully prepared the mixed conducting matrices, such as $FeF_3{\cdot}0.33H_2O/MoS_2$ [19], $FeF_3{\cdot}0.33H_2O/V_2O_5$ [20], $FeF_3{\cdot}0.33H_2O$/ACMB [21], $FeF_3$/G [22], $FeF_3{\cdot}xH_2O$/G [23], $Fe_2F_5{\cdot}H_2O$/G [24] and $Fe_2F_5{\cdot}H_2O$/rGO [25] cathode materials for LIBs and sodium ion batteries (SIBs), which showed some promising results. However, the capacity and cyclic property of $FeF_3{\cdot}0.33H_2O$/C nanocomposite are still required to be improved.

In addition, the substitution of elements such as Co [26], N [27] and -OH [28] for iron and fluorine elements is another effective strategy to improve the intrinsic electronic conductivity and crystal structural stability of $FeF_3$ cathode materials, thus it can evidently enhance their electrochemical performance. Generally, $TiF_3$ has the same crystal structure as $FeF_3$ and shows similar electrochemical activity [29,30]. In the studies of the LIBs cathode materials, Ti is usually applied as doping element due to its polyvalence and strong bond with nonmetalloid, but it has rarely been reported as the doping element of $FeF_3{\cdot}0.33H_2O$ [31–34]. In our previous work, the first-principles calculation was used to investigate the properties and electronic structures of Ti-doped $FeF_3{\cdot}0.33H_2O$, it can be found that the crystal volume of Ti doped $FeF_3{\cdot}0.33H_2O$ was slightly increased with the increase of Ti-doping concentration. The band gap of $FeF_3{\cdot}0.33H_2O$ and $Fe_{0.92}Ti_{0.08}F_3{\cdot}0.33H_2O$ is 0.78 eV and 0.66 eV, respectively. Therefore, the electronic conductivity of $FeF_3{\cdot}0.33H_2O$ can be improved by Ti doping. These results can be ascribed to the substitution of large radius $Ti^{3+}$ (6.70 Å) for small radius $Fe^{3+}$ (6.45 Å), which can enlarge the structure of the lattice crystal, thus resulting in improving the electrochemical performance of $FeF_3{\cdot}0.33H_2O$ cathode materials [35].

In this work, we report a facile strategy for the synthesis of Ti-doped $FeF_3{\cdot}0.33H_2O$/C nanocomposite as ultrahigh rate LIBs cathode material. The $Fe_{1-x}Ti_xF_3{\cdot}0.33H_2O$ ($x$ = 0, 0.06, 0.08, 0.10) nanocomposite was firstly synthesized via a liquid-phase followed by a low temperature reaction, then the $Fe_{1-x}Ti_xF_3{\cdot}0.33H_2O$/C ($x$ = 0, 0.06, 0.08, 0.10) nanocomposites were further obtained by mechanical ball-milling. Ball-milling is a facile and effective approach to synthesize the nanocomposite with superior conductivity, nevertheless, the mechanical force caused by grinding against each other will induce strain on the $FeF_3{\cdot}0.33H_2O$ crystals. The cycle performance of $FeF_3{\cdot}0.33H_2O$/C nanocomposite can be apparently improved after heat-treatment at a certain temperature, which is related to the release of the strain [36]. Moreover, with the combination of a carbon coating and Ti-doping, the as-prepared $Fe_{1-x}Ti_xF_3{\cdot}0.33H_2O$/C may remarkably improve the electrochemical performances as expected. The physicochemical and electrochemical properties of $Fe_{1-x}Ti_xF_3{\cdot}0.33H_2O$/C nanocomposite are studied in detail.

## 2. Experimental

### 2.1. Preparation of $Fe_{1-x}Ti_xF_3{\cdot}0.33H_2O$/C nanocomposite

The preparation of $Fe_{(1-x)}Ti_xF_3{\cdot}0.33H_2O$/C(x = 0, 0.06, 0.08, 0.10) nanocomposites are shown in Scheme 1. Iron(III) chloride hexahydrate ($FeCl_3{\cdot}6H_2O$) and titanium trichloride hexahydrate ($TiCl_3{\cdot}6H_2O$) in a molar ratio of 1.0:0, 0.94:0.06, 0.92:0.08 and 0.90:0.10 were dissolved in deionized water to gain a solution, respectively, then 10% excess mass of stoichiometric sodium hydroxide (NaOH) solution was dropwise added to the solution under vigorous stirring to form $Fe_{1-x}Ti_x(OH)_3$ precipitations. The obtained $Fe_{1-x}Ti_x(OH)_3$ precipitations were aged for 36 h, filtered, washed with deionized water, dried at 80 °C for 6 h in the air to remove redundant water. Then, 20 mL hydrofluoric acid (HF) aqueous solution (40 wt%) was dropwise added into the above precipitations tardily in a Teflon-lined stainless steel autoclave with continued stirring for 12 h to obtain a uniform pink liquid, then the solution was continuously agitated at 80 °C for 12 h to form pink precipitates. Then mixture was heated at 80 °C in the open autoclave for another 12 h in order to remove the remaining HF and water. Subsequently, the residue in bottle was further dried at 80 °C in vacuum to obtain the $Fe_{1-x}Ti_xF_3$ $3H_2O$ precursor, and the as-prepared precursor was heated at tube furnace (220 °C for 8 h) in high-purity argon to remove the crystal water and changed into $Fe_{1-x}Ti_xF_3{\cdot}0.33H_2O$. Next, $Fe_{1-x}Ti_xF_3{\cdot}0.33H_2O$ and carbon black (AB) (85:15 wt/wt) were milled in a high energy ball grinding mill at 300 rpm for 3 h, the as-prepared mixture was converted into $Fe_{1-x}Ti_xF_3{\cdot}0.33H_2O$/C nanocomposites. Finally, the prepared $Fe_{1-x}Ti_xF_3{\cdot}0.33H_2O$/C composites were dried at tube furnace (220 °C for 3 h) in high-purity argon to obtain the products. Actually, in this work the $Fe_{1-x}Ti_xF_3{\cdot}0.33H_2O$/C nanocomposites have a content of 10% Ti, the Fe position is partially replaced by Ti in the $FeF_3{\cdot}0.33H_2O$/C crystal. In the related literature [26,37,38], the materials with similar doping levels are usually treated as doping material. The diagram of Ti-doping is shown in Scheme 1. As shown in Scheme 1, the atomic structure of Ti doped $FeF_3{\cdot}0.33H_2O$ was also schematically given. The blue ball refers to O atom, the yellow ball refers to H atom, the olive ball refers to F atom, the lilac ball refers to Fe atom and the red ball refers to Ti atom.

### 2.2. Structural characterizations

To observe the particle size and morphologies of the $Fe_{1-x}Ti_xF_3{\cdot}0.33H_2O$ and $Fe_{1-x}Ti_xF_3{\cdot}0.33H_2O$/C samples, the scanning electron microscope (SEM, JEOL JSM-6610LV) and transmission electron microscopy (TEM, JEOL JEM-2100F) were used. Further structural characterization and elemental distribution of the materials were carried out by high-resolution TEM (HRTEM, JEOL JEM-2100F) at an acceleration voltage of 200 kV equipped with an energy dispersive an energy-dispersive X-ray spectroscope (EDXS) (JSM-6100LV, JEOL, Japan) detector. To observe the crystalline phase of the samples, The X-ray diffraction (XRD) data were obtained using an X-ray diffractometer (Bruker AXS D8, Bruker AXS GmbH, Germany), equipped with Cu Kα radiation (λ = 0.154178 nm) and a graphite monochromator, in the diffracting angular range (2θ) range of 10°–80° at a continuous scan mode with a scan rate of 4° $min^{-1}$.

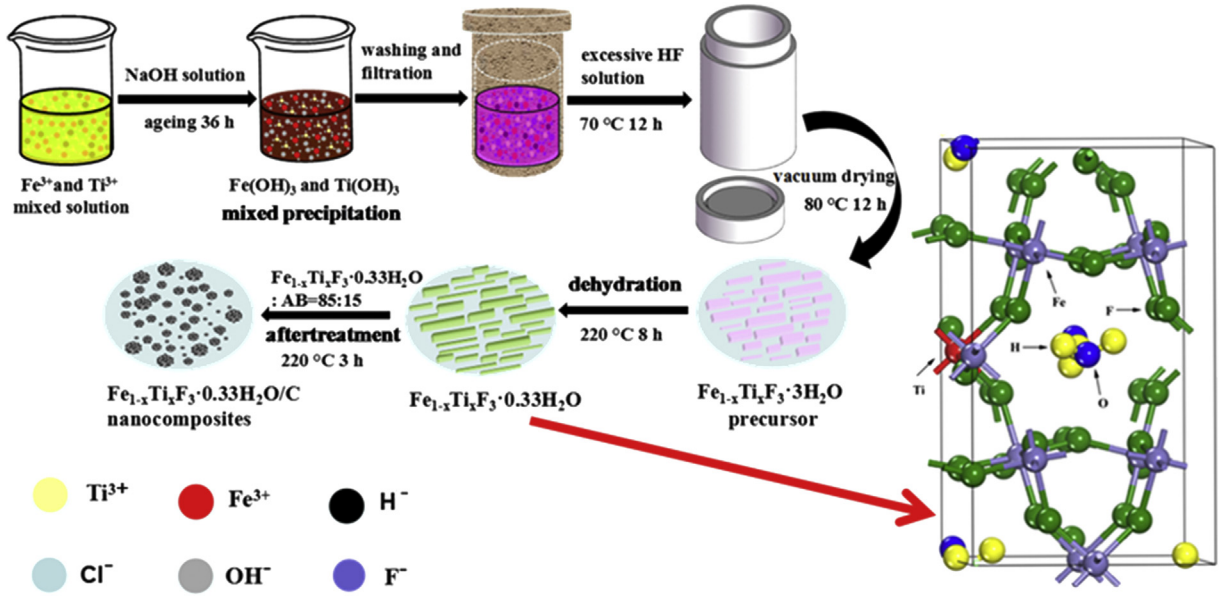


**Scheme 1.** The schematic representation of $Fe_{1-x}Ti_xF_3{\cdot}0.33H_2O$/C nanocomposite preparation; (insert) $FeF_3{\cdot}0.33H_2O$ doped by one Ti atom.

### 2.3. Electrochemical measurements

The electrochemical performance of the as-synthesized material was characterized using 2025 type coin cells, in which $Fe_{1-x}Ti_xF_3{\cdot}0.33H_2O$/C nanocomposite was used as a cathode active material and a lithium disk as cathode for LIBs. The cathodes for testing cells were fabricated by mixing the cathode materials, acetylene black, and polyvinylidene fluoride (PVDF) binder with a weight ratio of 80:10:10 in N-methyl pyrrolidione (NMP), which were then pasted on aluminum foil followed by drying under vacuum at 110 °C for 24 h. The testing lithium cells were assembled with the cathode thus fabricated, metallic lithium anode, Celgard 2300 film separator, and 1 mol $L^{-1}$ $LiPF_6$ in 1:1 ethylene carbonate (EC)/dimethyl carbonate (DMC) electrolyte. The assembly of the testing cells was carried out in an argon-filled glove box, where water and oxygen concentration were kept less than 5 ppm. The charge/discharge cycle tests for LIBs were conducted at different current densities on the Neware battery tester BTS-XWJ-6.44S-00052 (Neware, Shenzhen, China) between 1.5 and 4.5 V. The assembly of cells were allowed to age for 12 h before testing. The cyclic voltammogram (CV) was performed at a scan rate of 0.1 mV $s^{-1}$ on the potential interval 1.5–4.5 V (vs. $Li^+$/Li) by an electrochemical workstation (VersaSTAT3, Princeton Applied Research). Electrochemical impedance spectroscopy (EIS) was also performed using VersaSTAT3 electrochemical workstation by applying an ac amplitude of 1 mV over the frequency range from $10^{-2}$–$10^5$ Hz. All the electrochemical measurements were carried out at room temperature.

## 3. Results and discussion

Fig. 1a–d shows the apparent morphologies of $Fe_{1-x}Ti_xF_3{\cdot}0.33H_2O$ (after calcination, before ball-milling), while Fig. 1e–h represent $Fe_{1-x}Ti_xF_3{\cdot}0.33H_2O$/C (after ball-milling with AB) nanocomposite. As shown in Fig. 1a–d, it can be found that all the $Fe_{1-x}Ti_xF_3{\cdot}0.33H_2O$ samplles are a cuboid appearance with the size of (3–7 μm). The particles of $FeF_3{\cdot}0.33H_2O$ are glossy, while the surfaces of $Fe_{1-x}Ti_xF_3{\cdot}0.33H_2O$ particles become increasingly rough, and some tiny particles are attached on the surface of the cuboid particles with the increase of Ti dopant amount. It is well known that the rough surface is beneficial to the electrolyte permeation and the electrochemical performance enhancement [39–42]. After ball-milling with AB, the particle sizes of the $Fe_{1-x}Ti_xF_3{\cdot}0.33H_2O$/C are reduced to nano scale (100–500 nm), and the morphology changes from cuboid into irregular crystal shape due to aggregation, as shown in Fig. 1e–h. In addition, the particle size of $FeF_3{\cdot}0.33H_2O$/C is larger than other Ti-doped samples, and $Fe_{0.92}Ti_{0.08}F_3{\cdot}0.33H_2O$ composite shows the most uniform particle size distribution. Of course, smaller size $Fe_{1-x}Ti_xF_3{\cdot}0.33H_2O$/C particles can increase the specific surface area and reduce the ion diffusion distance. Besides, the conductive carbon, distributed uniformly on the surface of the nanocomposite, is also beneficial to enhance the electronic conductivities and thus improving the electrochemical performances [43].

The effects of Ti-doping on the performances of the samples were discussed sufficiently by XRD, EDXs and EIS. It has been reported by Li et al. [16] that the low content of hydration water in $FeF_3{\cdot}0.33H_2O$ is indispensable because it serves as a structural stabilizer. Fig. 2a shows the XRD patterns of $Fe_{1-x}Ti_xF_3{\cdot}0.33H_2O$/C nanocomposites ($x$ = 0.00, 0.06, 0.08, 0.10). All samples show intensive peaks at 2θ = 13.8°, 23.6° and 27.8° accord with (110), (002) and (220) diffraction peaks of $FeF_3{\cdot}0.33H_2O$. The main diffraction peaks are appeared at similar position, which are in good agreement with the standard peaks of $FeF_3{\cdot}0.33H_2O$ (orthorhombic structure with *Cmcm* space group, JCPDS No. 76-1262). No carbon peak for the $Fe_{1-x}Ti_xF_3{\cdot}0.33H_2O$/C composites is detected since the AB is amorphous [15,26]. In addition, the absence of distinct Ti diffractions in $Fe_{1-x}Ti_xF_3{\cdot}0.33H_2O$/C indicates that Ti is doped effectively and does not change the structure of $FeF_3{\cdot}0.33H_2O$ fundamentally.

The diffraction peak at around 2θ = 13.8° shifts to a smaller angle as the titanium content increases, which suggests that titanium substitution expands the interplanar spacing of the (110) planes (Fig. 2a) because the radius of the $Ti^{3+}$ ion (6.70 Å) is slightly larger than that of the $Fe^{3+}$ ion (6.45 Å), but less than that of $Li^+$ ion (6.8 Å) [35,43]. As a result, the partial $Ti^{3+}$ replacement for $Fe^{3+}$ in $FeF_3{\cdot}0.33H_2O$ crystal can cause the expansion of crystal lattice. Lattice expansion will enlarge the pathway and weaken the lattice resistance to $Li^+$ ion diffusion [35], as predicted by our previous first-principles calculations, thus improving the rate capacity of

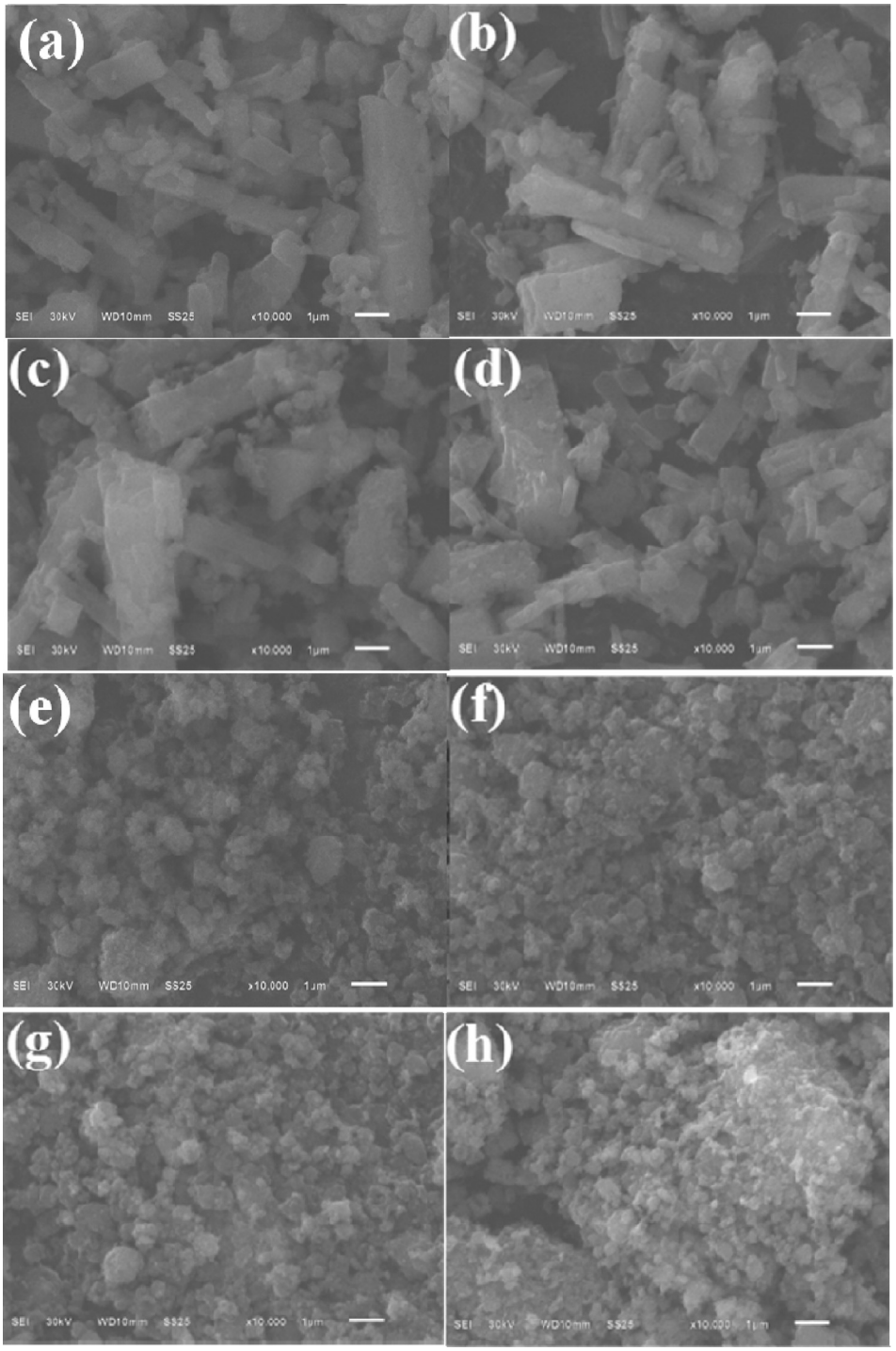


**Fig. 1.** (a) SEM images of $FeF_3{\cdot}0.33H_2O$; (b) $Fe_{0.94}Ti_{0.06}F_3{\cdot}0.33H_2O$; (c) $Fe_{0.92}Ti_{0.08}F_3{\cdot}0.33H_2O$; (d) $Fe_{0.90}Ti_{0.10}F_3{\cdot}0.33H_2O$; (e) $FeF_3{\cdot}0.33H_2O$/C; (f) $Fe_{0.94}Ti_{0.06}F_3{\cdot}0.33H_2O$/C; (g) $Fe_{0.92}Ti_{0.08}F_3{\cdot}0.33H_2O$/C, and (h) $Fe_{0.90}Ti_{0.10}F_3{\cdot}0.33H_2O$/C composite.

$Fe_{1-x}Ti_xF_3{\cdot}0.33H_2O$/C nanocomposite, which are further confirmed by the following electrochemical performances.

The crystallographic view of orthorhombic $FeF_3{\cdot}0.33H_2O$ along the direction of [001] was illustrated in Fig. 2c, as being seen, there is a special huge hexagonal cavity formed six Fe octahedral via corner-sharing, which can result in a larger cell volumes (~71 nm). The trace amount of water in $FeF_3{\cdot}0.33H_2O$ exist stably in the huge hexagonal cavity, it can be used as a structural stabilizer to stabilize the huge hexagonal cavity and avoid structure collapse during $Li^+$ insertion and extraction processes [15,26]. Therefore, $FeF_3{\cdot}0.33H_2O$ provide the space for accommodation and transport $Li^+$.

The TEM and HRTEM are performed to accurately observed the morphology and detailed crystal structures of as-prepared materials. It can be clearly seen in Fig. 3a that the $Fe_{0.92}Ti_{0.08}F_3{\cdot}0.33H_2O$/C nanocomposite is composed of large clusters, which is made of many smaller particles. As illustrated in Fig. 3b, HRTEM images shows that the $Fe_{0.92}Ti_{0.08}F_3{\cdot}0.33H_2O$ (2–6 nm) nanocrystalline is encapsulated by an amorphous carbon matrix after ball milling.

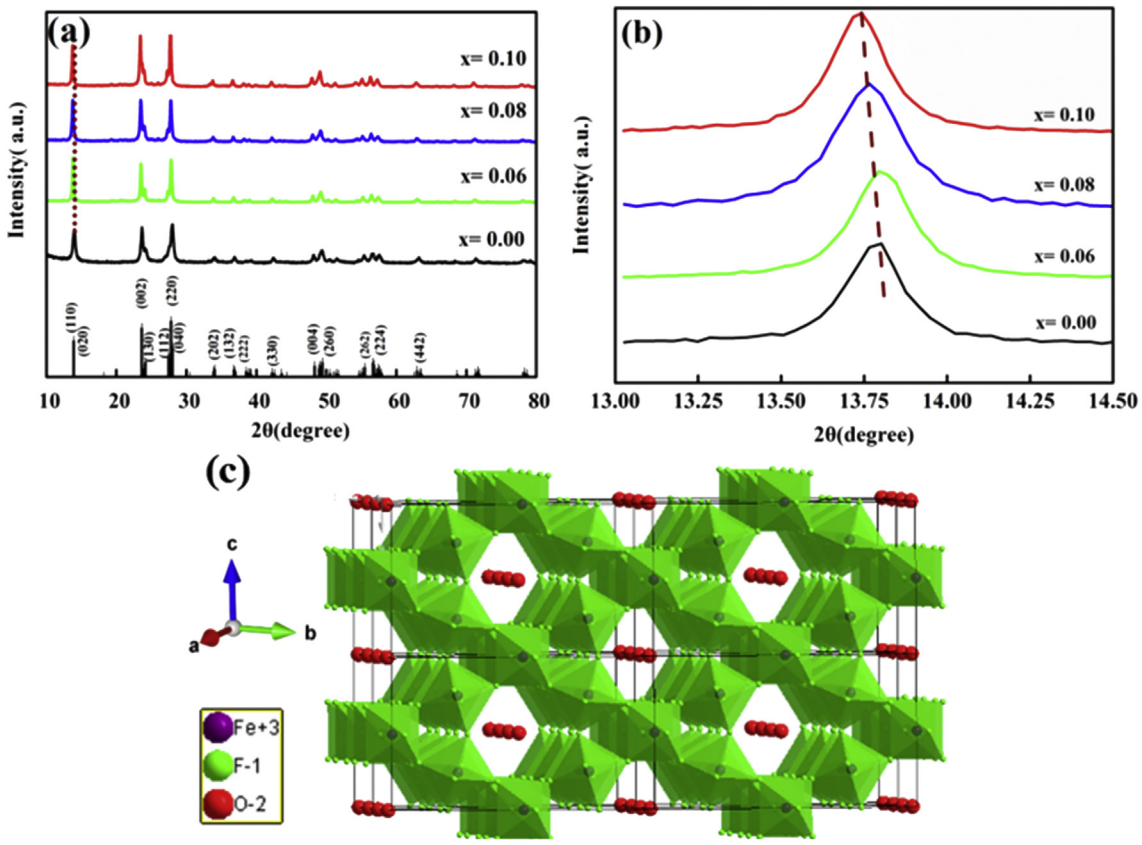


**Fig. 2.** (a) XRD patterns of $Fe_{1-x}Ti_xF_3 \cdot 0.33H_2O$/C (x = 0, 0.06, 0.08, 0.10) nanocomposites; (b) Magnification of the (110) XRD peak at around 2θ = 13.8°; (c) Projections of $FeF_3 \cdot 0.33H_2O$ along the direction of [001].

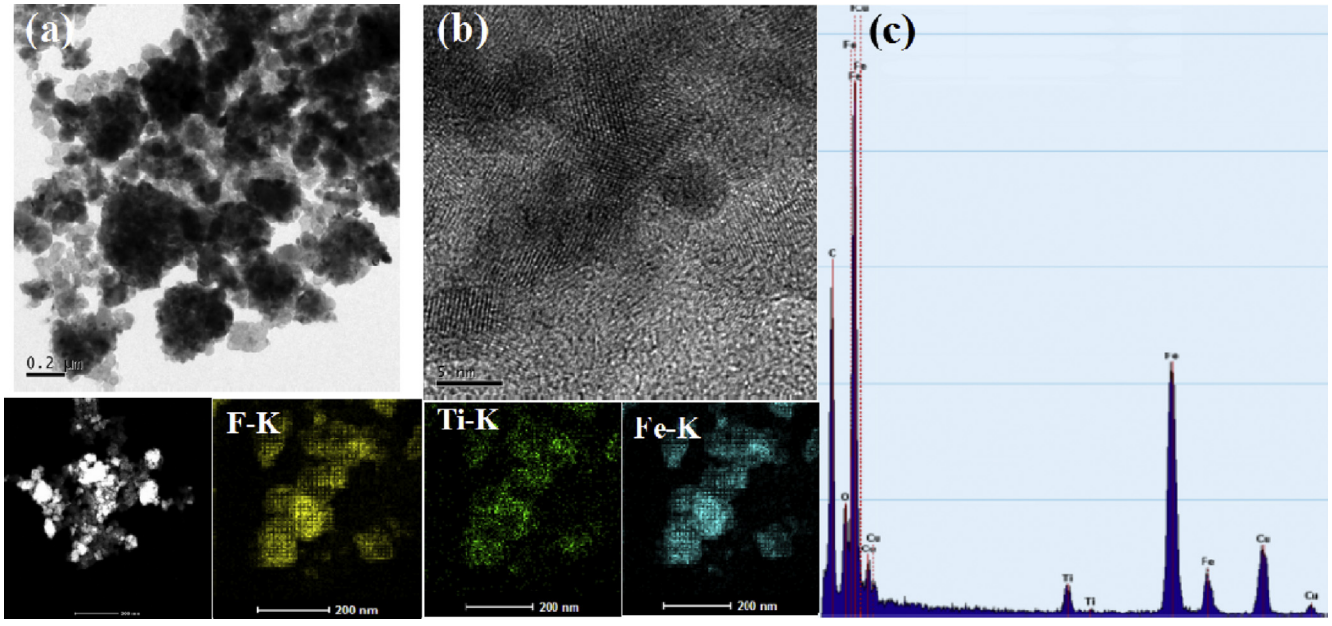


**Fig. 3.** (a) TEM and (b) HRTEM images of $Fe_{0.92}Ti_{0.08}F_3 \cdot 0.33H_2O$/C nanocomposite, (c) EDXs spectrum (c) and corresponding EDXs mapping images (F, Ti and Fe) of $Fe_{0.92}Ti_{0.08}F_3 \cdot 0.33H_2O$/C nanocomposite.

Besides, $Fe_{0.92}Ti_{0.08}F_3 \cdot 0.33H_2O$/C nanocomposite has the smallest particle size and best network structure, which is considered to be in favor of electrolyte penetration into the electrode and it can provide more interface between the electrode material and the electrolyte. In order to further investigate the elemental distributions and compositions of the $Fe_{0.92}Ti_{0.08}F_3 \cdot 0.33H_2O$/C nanocomposite, the TEM images and corresponding EDXs mappings are shown in Fig. 3c. The Cu peaks come from a copper collector. The

average molar ratios for Fe, Ti, and F (Fe: 0.912, Ti: 0.077, F: 2.928) are in agreement with the nominal ratios. The result indicates that the Ti ions have been completely introduced into the $FeF_3 \cdot 0.33H_2O$/C nanocomposite via liquid phase method.

To further investigate the reason of improvement in the electrochemical performance for Ti-doping, the EIS analysis of $Fe_{1-x}Ti_xF_3 \cdot 0.33H_2O$/C nanocomposites (x = 0.0, 0.08) is carried out, as shown in Fig. 4a and b. The shapes of the Nyquist plots for each cycle are similar. The EIS is recorded during 1st to 100$^{th}$ charge/discharge cycles at room temperature. The EIS pattern is composed of a semicircle within high-frequency region and a sloped straight line at low-frequency region. The semicircle is mainly ascribed to the charge transfer resistance ($R_{ct}$), which reflects the reaction kinetics of the electrodes; while the sloping line represent the Warburg impedance ($Z_w$), which is related to lithium ion diffusion in the solid matrix. The corresponding equivalent circuit model is shown in Fig. 4c, apparently, the fitting patterns are in good agreement with the experimental EIS data. As shown in Table 1, it can be found that the $R_s$ value for all electrodes is almost the same. Besides, the $R_{ct}$ values of $FeF_3 \cdot 0.33H_2O$/C electrode at different cycle numbers are 220.4, 285.0, 449.3 Ω at 1st, 50$^{th}$, 100$^{th}$ cycles, respectively. By contrast, the $R_{ct}$ values for the $Fe_{0.92}Ti_{0.08}F_3 \cdot 0.33H_2O$/C electrode after 1st, 50$^{th}$, 100$^{th}$ cycles are 195.9, 263.3, 319.1 Ω, respectively. Thereby, the introduction of Ti can effectively decrease the charge transfer resistance and thus enhance the electrochemical performance of iron based fluoride cathode material. It can be found from Table 1 that the $R_{ct}$ value of $Fe_{0.92}Ti_{0.08}F_3 \cdot 0.33H_2O$/C nanocomposite is less than that of $FeF_3 \cdot 0.33H_2O$/C nanocomposite, implying that the $Fe_{0.92}Ti_{0.08}F_3 \cdot 0.33H_2O$/C nanocomposite has higher conductivity and faster lithium ion diffusion kinetics than $FeF_3 \cdot 0.33H_2O$/C sample.

The 1st and 40$^{th}$ charge/discharge profiles of $Fe_{1-x}Ti_xF_3 \cdot 0.33H_2O$/C nanocomposites (x = 0.00, 0.06, 0.08, 0.10) are recorded at 0.1 C (1 C = 237 mA g$^{-1}$) rate in the voltage range of 1.5–4.5 V (vs. $Li^+$/Li), as shown in Fig. 5a–d. The $FeF_3 \cdot 0.33H_2O$/C electrode delivers a low initial discharge capacity of 299.98 mAh g$^{-1}$, which is attributed to its poor electronic conductivity. Obviously, the Ti-doped materials show higher discharge capacity than

**Table 1**
$R_s$ and $R_{ct}$ values of $FeF_3 \cdot 0.33H_2O$/C and $Fe_{0.92}Ti_{0.08}F_3 \cdot 0.33H_2O$/C samples after different cycles in Li half-cells.

| Samples | $FeF_3 \cdot 0.33H_2O$/C | | | $Fe_{0.92}Ti_{0.08}F_3 \cdot 0.33H_2O$/C | | |
|---|---|---|---|---|---|---|
| Cycles | 1$^{st}$ | 50$^{th}$ | 100$^{th}$ | 1$^{st}$ | 50$^{th}$ | 100$^{th}$ |
| $R_s$(Ω) | 5.999 | 6.151 | 6.350 | 2.140 | 2.391 | 2.568 |
| $R_{ct}$(Ω) | 220.4 | 285.0 | 449.3 | 195.9 | 265.3 | 319.1 |

$FeF_3 \cdot 0.33H_2O$/C. The initial discharge capacities when x = 0.06, 0.08, 0.10 are 361.70 mAh g$^{-1}$, 460.15 mAh g$^{-1}$, 399.48 mAh g$^{-1}$, respectively, thus Ti-doping with an optimal content can improve the specific capacity. Particularly, $Fe_{0.92}Ti_{0.08}F_3 \cdot 0.33H_2O$/C delivers the highest specific capacity and exhibits an excellent cycling performance compared with other three nanocomposite. In addition, the $Fe_{0.92}Ti_{0.08}F_3 \cdot 0.33H_2O$/C nanocomposite exhibits also the highest discharge voltage plateau and lowest charge voltage plateau from the 1st to the 40$^{th}$ cycles. As shown in Fig. 5e, the $Fe_{0.92}Ti_{0.08}F_3 \cdot 0.33H_2O$/C cell shows excellent cycling performance, it can provide an initial discharge capacity of 460.15 mAh g$^{-1}$ at 0.1 C and a discharge capacity of 294.86 mAh g$^{-1}$ after 40 cycles. By contrast, the $FeF_3 \cdot 0.33H_2O$/C cell can reach an initial discharge capacity of 299.98 mAh g$^{-1}$ at 0.1 C, but the discharge capacity of $FeF_3 \cdot 0.33H_2O$/C is only 162.66 mAh g$^{-1}$ after 40 cycles. In addition, the voltage fading of $Fe_{0.92}Ti_{0.08}F_3 \cdot 0.33H_2O$/C cell is distinctly lower than $FeF_3 \cdot 0.33H_2O$/C cell with the increase of the cycle number. As expected, the discharge specific capacity of the nanocomposites is superior to those of the recently reported results. For example, Rao et al. prepared $FeF_3.0.33H_2O$/rGO composite via a solvothermal route and obtained a discharge capacity of 165.0 mAh g$^{-1}$ at 0.1 C after 30 cycles [44]. Xu et al. synthesized $FeF_3 \cdot 0.33H_2O$/C nanocomposite by one-step solid state method, and it only maintained a low discharge capacity of 157.4 mAh g$^{-1}$ at 20 mA g$^{-1}$ after 50 cycles [45]. Apparently, the $Fe_{1-x}Ti_xF_3 \cdot 0.33H_2O$/C nanocomposite in this work exhibits much better excellent electrochemical performances.

In addition to the excellent cycling performance, the $Fe_{0.92}Ti_{0.08}F_3 \cdot 0.33H_2O$/C cell displays also good rate capability compared

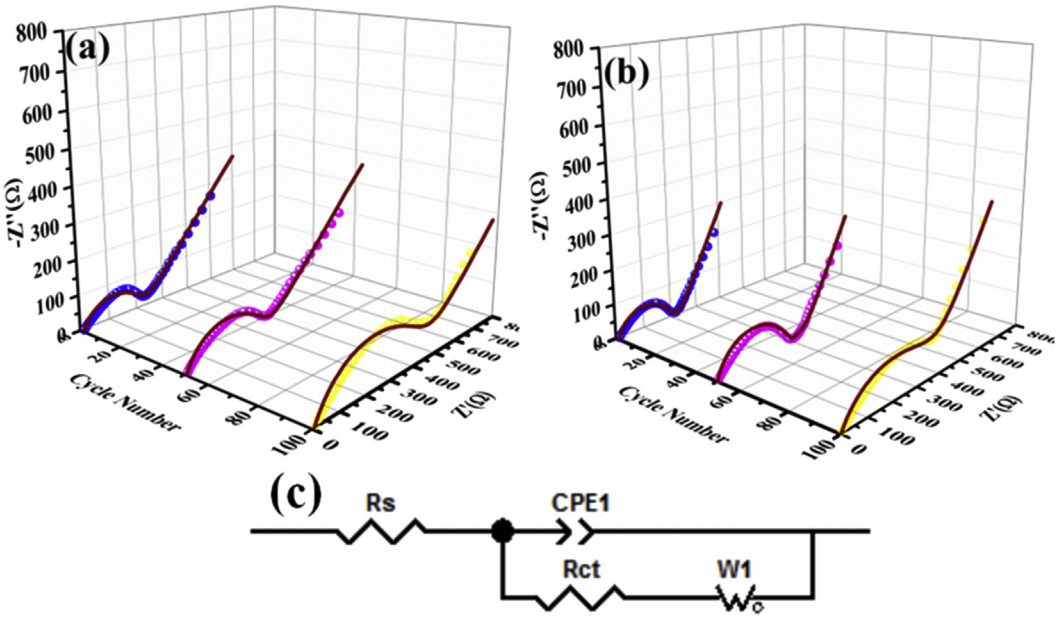


**Fig. 4.** Three-dimensional Nyquist plots measured for (a) $FeF_3 \cdot 0.33H_2O$/C and (b) $Fe_{0.92}Ti_{0.08}F_3 \cdot 0.33H_2O$/C samples after cycling for different cycles at 1 C in Li half-cells; (c) the equivalent circuit model.

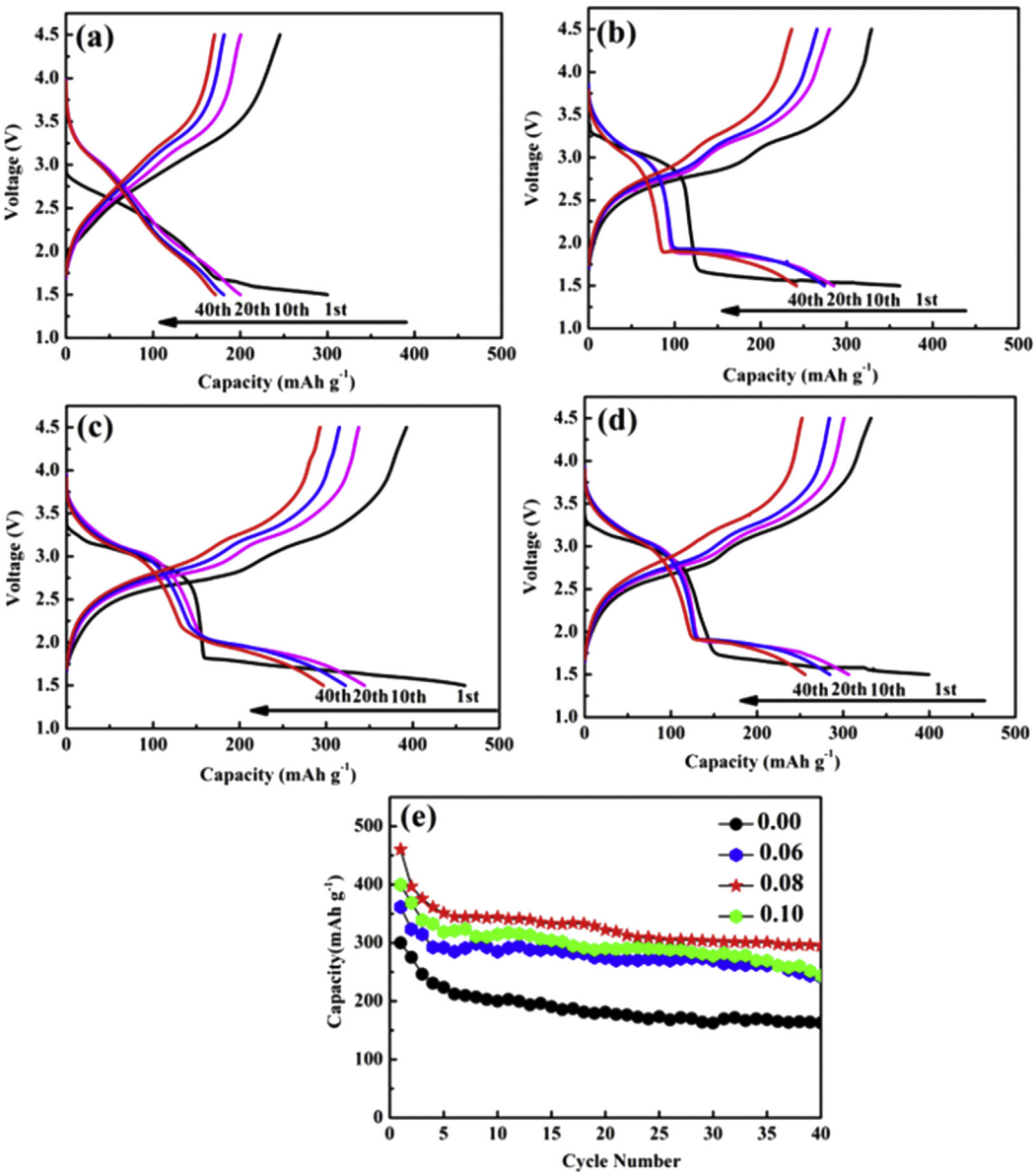


**Fig. 5.** Discharge and charge profiles of (a) $FeF_3 \cdot 0.33H_2O$/C; (b) $Fe_{0.94}Ti_{0.06}F_3 \cdot 0.33H_2O$/C; (c) $Fe_{0.92}Ti_{0.08}F_3 \cdot 0.33H_2O$/C; (d) $Fe_{0.90}Ti_{0.10}F_3 \cdot 0.33H_2O$/C; at 0.1C at different cycles (1st, 10th, 20th, 40$^{th}$); (e) Discharge capacity vs. cycle number for 0.00, 0.06, 0.08, 0.10 at 0.1 C in the voltage range of 1.5–4.5 V.

with the $FeF_3 \cdot 0.33H_2O$/C cell. As illustrated in Fig. 6a, the rate capabilities of the $Fe_{0.92}Ti_{0.08}F_3 \cdot 0.33H_2O$/C and $FeF_3 \cdot 0.33H_2O$/C nanocomposite are examined at 0.1 C, 0.2 C, 0.5 C, 1 C and 2 C rates for 10 cycles, respectively. The initial discharge capacity of $Fe_{0.92}Ti_{0.08}F_3 \cdot 0.33H_2O$/C cell can reach as high as 470.51 mAh g$^{-1}$ at 0.1 C. The average discharge capacity of $Fe_{0.92}Ti_{0.08}F_3 \cdot 0.33H_2O$/C cell is 366.06 mAh g$^{-1}$ at 0.1 C. And the subsequent average discharge capacity are about 314.34 mAh g$^{-1}$, 257.92 mAh g$^{-1}$ 200.25 mAh g$^{-1}$ and 146.06 mAh g$^{-1}$ at rate of 0.2 C, 0.5 C,1 C and 2 C, respectively. Apparently, with increasing C-rate, $Fe_{0.92}Ti_{0.08}F_3 \cdot 0.33H_2O$/C gives much higher discharge capacity and much better rate capability than $FeF_3 \cdot 0.33H_2O$/C. Additionally, there is a slight capacity fading for the $FeF_3 \cdot 0.33H_2O$/C electrode when the current density decreases from 2 C to 0.1 C, but the capacity of the $Fe_{0.92}Ti_{0.08}F_3 \cdot 0.33H_2O$/C electrode can be recovered quickly. When the rate backs to 0.1 C after 50 cycles, a capacity of 261.74 mA h g$^{-1}$ can be resumed.

To further study the cycling performance of $FeF_3 \cdot 0.33H_2O$/C and $Fe_{0.75}Ti_{0.25}F_3 \cdot 0.33H_2O$/C electrodes at high rate, the samples were cycled at 1 C in the voltage range of 1.5–4.5 V, as shown in Fig. 6b–d. It can be found that a discharge capacity of 179.62 mA h g$^{-1}$ can be remained after 60 cycles for the $Fe_{0.92}Ti_{0.08}F_3 \cdot 0.33H_2O$/C electrode and the capacity retention is 85.9%. On the contrary, the $FeF_3 \cdot 0.33H_2O$/C electrode suffers a fast capacity fading and it only delivers 144.54 mA h g$^{-1}$ with a capacity retention of 72.2% after 60 cycles. The good electrochemical performance of $Fe_{0.92}Ti_{0.08}F_3 \cdot 0.33H_2O$/C electrodes is probably due to the large increase of the lattice parameters after Ti doping, which can enhance the diffusion coefficient of $Li^+$ and lower the activation barrier of $Li^+$ diffusion with the increasing current rate. In addition, the Ti substitution for Fe can also stabilize the crystal structure of the material, which can provide a stable pathway for $Li^+$ to both insertion and conversion reactions [46,47].

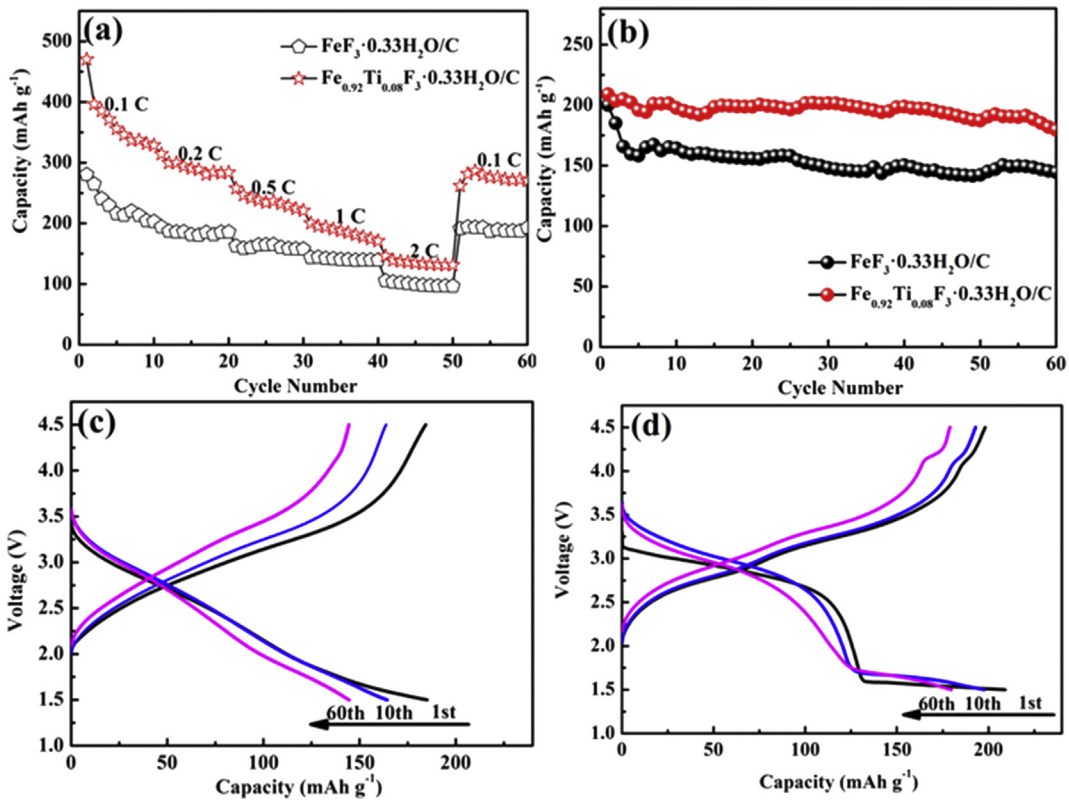


**Fig. 6.** Rate capabilities of (a) $FeF_3 \cdot 0.33H_2O/C$ and $Fe_{0.92}Ti_{0.08}F_3 \cdot 0.33H_2O/C$ electrodes; (b) the discharge capacity *vs.* cycle number for $FeF_3 \cdot 0.33H_2O/C$ and $Fe_{0.92}Ti_{0.08}F_3 \cdot 0.33H_2O/C$ electrodes at 1 C in the voltage range of 1.5–4.5 V; the charge/discharge curves of the (c) $FeF_3 \cdot 0.33H_2O/C$ and (d) $Fe_{0.92}Ti_{0.08}F_3 \cdot 0.33H_2O/C$ cells at particular cycles.

## 4. Conclusions

$Fe_{1-x}Ti_xF_3 \cdot 0.33H_2O$ has been successfully prepared through a simple liquid-phase method and followed by a heat-treatment process, and then mixed with carbon black by ball-milling to obtain $Fe_{1-x}Ti_xF_3 \cdot 0.33H_2O/C$ nanocomposite as cathode materials of LIBs. Smaller particles size, faster lithium ion diffusion rate and less polarization confer the Ti-doped $FeF_3 \cdot 0.33H_2O/C$ nanocomposite outstanding electrochemical performance. Moreover, Ti can effectively and equably doped into $FeF_3 \cdot 0.33H_2O$ crystal, and replace partially $Fe^{3+}$ site in the $FeF_3 \cdot 0.33H_2O$ crystal. Ti-doping can not only decrease apparently the charge transfer resistance of $FeF_3 \cdot 0.33H_2O/C$, but also notably enhance the discharge capacity and cycling stability. Especially, the $Fe_{0.92}Ti_{0.08}F_3 \cdot 0.33H_2O/C$ material exhibits a highest initial discharge specific capacity of 460.15 mAh g$^{-1}$ and retains a discharge capacity of 294.86 mAh g$^{-1}$ after 40 cycles at 0.1 C among all samples. In addition, the $Fe_{0.92}Ti_{0.08}F_3 \cdot 0.33H_2O/C$ nanocomposite also shows good excellent rate capability, it can provide a discharge capacity of 146.06 mAh g$^{-1}$ even at 2 C. Therefore, Ti-doping will be of general interest and contribute meaningful guidance for designing high performance metal fluoride cathode for LIBs.

## Acknowledgements

This work is supported financially by the National Natural Science Foundation of China under project No. 51472211 and No. 21573187, Key Project of Strategic New Industry of Hunan Province under project No. 2016GK4005 and 2016GK4030.

## References

[1] F. Badway, N. Pereira, F. Cosandey, G.G. Amatucci, Carbon-metal fluoride nanocomposites structure and electrochemistry of $FeF_3$:C, J. Electrochem. Soc. 150 (2003) A1209–A1218.
[2] H. Arai, S. Okada, Y. Sakurai, J. Yamaki, Cathode performance and voltage estimation of metal trihalides, J. Power Sources 68 (1997) 716–719.
[3] R.E. Doe, K.A. Persson, Y.S. Meng, G. Ceder, First-principles investigation of the Li-Fe-F phase diagram and equilibrium and nonequilibrium conversion reactions of iron fluorides with lithium, Chem. Mater. 20 (2008) 5274–5283.
[4] S.W. Kim, D.H. Seo, H. Gwon, J. Kim, K. Kang, Fabrication of $FeF_3$ nanoflowers on CNT branches and their application to high power lithium rechargeable batteries, Adv. Mater. 22 (2010) 5260–5264.
[5] F. Badway, F. Cosandey, N. Pereira, G.G. Amatucci, Carbon metal fluoride nanocomposites high-capacity reversible metal fluoride conversion materials as rechargeable positive electrodes for Li batteries, J. Electrochem. Soc. 150 (2003) A1318–A1327.
[6] T. Li, L. Li, Y.L. Cao, X.P. Ai, H.X. Yang, Reversible three-electron redox behaviors of $FeF_3$ nanocrystals as high-capacity cathode-active materials for Li-Ion batteries, J. Phys. Chem. C 114 (2010) 3190–3195.
[7] M. Nishijima, I.D. Gocheva, S. Okada, T. Doi, J. Yamaki, T. Nishida, Cathode properties of metal trifluorides in Li and Na secondary batteries, J. Power Sources 190 (2009) 558–562.
[8] J.L. Tan, L. Liu, H. Hu, Z.H. Yang, H.P. Guo, Q.L. Wei, X. Yi, Z.C. Yan, Q. Zhou, Z.F. Huang, H.B. Shu, X.K. Yang, X.Y. Wang, Iron fluoride with excellent cycle performance synthesized by solvothermal method as cathodes for lithium ion batteries, J. Power Sources 251 (2014) 75–84.
[9] Q.X. Chu, Z.C. Xing, J.Q. Tian, X.B. Ren, A.M. Asiri, A.O. Al-Youbi, K.A. Alamry, X.P. Sun, Facile preparation of porous $FeF_3$ nanospheres as cathode materials for rechargeable lithium-ion batteries, J. Power Sources 236 (2013) 188–191.
[10] F. Badway, A.N. Mansour, N. Pereira, J.F. Al-Sharab, F. Cosandey, I. Plitz, G.G. Amatucci, Structure and electrochemistry of copper fluoride nanocomposites utilizing mixed conducting matrices, Chem. Mater. 19 (2007) 4129–4141.
[11] T. Li, L. Li, Y.L. Cao, X.P. Ai, H.X. Yang, Reversible three-electron redox behaviors of $FeF_3$ nanocrystals as high-capacity cathode-active materials for Li-Ion batteries, J. Phys. Chem. A 114 (2010) 3190–3195.
[12] C.L. Li, C.L. Yin, L. Gu, R.E. Dinnebier, X.K. Mu, P.A. van Aken, J. Maier, An $FeF_3 \cdot 0.5H_2O$ polytype: a microporous framework compound with intersecting tunnels for Li and Na batteries, J. Am. Chem. Soc. 135 (2013) 11425–11428.
[13] C.L. Li, C.L. Yin, X.K. Mu, J. Maier, Top-down synthesis of open framework fluoride for lithium and sodium batteries, Chem. Mater. 25 (2013) 962–969.
[14] C.L. Li, L. Gu, S. Tsukimoto, P.A. van Aken, J. Maier, Low-temperature ionic-liquid-based synthesis of nanostructured iron-based fluoride cathodes for lithium batteries, Adv. Mater. 22 (2010) 3650–3654.

[15] C.L. Li, L. Gu, J.W. Tong, S. Tsukimoto, J. Maier, A mesoporous iron-based fluoride cathode of tunnel structure for rechargeable lithium batteries, Adv. Funct. Mater. 21 (2011) 1391–1397.
[16] C.L. Li, L. Gu, J.W. Tong, J. Maier, Carbon nanotube wiring of electrodes for high-rate lithium batteries using an imidazolium-based ionic liquid precursor as dispersant and binder: a case study on iron fluoride nanoparticles, ACS Nano 5 (2011) 2930–2938.
[17] C.L. Li, X.K. Mu, P.A. van Aken, J. Maier, A high-capacity cathode for lithium batteries consisting of porous microspheres of highly amorphized iron fluoride densified from its open parent phase, Adv. Energy Mater. 3 (2013) 113–119.
[18] D.L. Ma, Z.Y. Cao, H.G. Wang, X.L. Huang, L.M. Wang, X.B. Zhang, Three-dimensionally ordered macroporous $FeF_3$and its *in situ* homogenous polymerizationcoating for high energy and power density lithium ion batteries, Energy Environ. Sci. 5 (2012) 8538–8542.
[19] W. Wu, X.Y. Wang, X. Wang, S.Y. Yang, X.M. Liu, Q.Q. Chen, Effects of $MoS_2$ doping on the electrochemical performance of $FeF_3$ cathode materials for lithium-ion batteries, Mater. Lett. 63 (2009) 1788–1790.
[20] W. Wu, Y. Wang, X.Y. Wang, Q.Q. Chen, X. Wang, S.Y. Yang, X.M. Liu, J. Guo, Z.H. Yang, Structure and electrochemical performance of $FeF_3/V_2O_5$composite cathode material for lithium-ion battery, J. Alloys. Compd. 486 (2009) 93–96.
[21] L. Liu, M. Zhou, X.Y. Wang, Z.H. Yang, F.H. Tian, X.Y. Wang, Synthesis and electrochemical performance of spherical $FeF_3$/ACMB composite as cathode material for lithium-ion batteries, J. Mater. Sci. 47 (2012) 1819–1824.
[22] Y.Q. Shen, X.Y. Wang, H. Hu, M.L. Jiang, Y.S. Bai, X.K. Yang, H.B. Shu, Sheet-like structure $FeF_3$/graphene composite as novel cathode material for Na ion batteries, RSC Adv. 5 (2015) 38277–38282.
[23] Y.Q. Shen, X.Y. Wang, H. Hu, M.L. Jiang, X.K. Yang, H.B. Shu, A graphene loading heterogeneous hydrated forms iron based fluoride nanocomposite as novel and high-capacity cathode material for lithium/sodium ion batteries, J. Power Sources 283 (2015) 204–210.
[24] M.L. Jiang, X.Y. Wang, Y.Q. Shen, H. Hu, Y.Q. Fu, X.K. Yang, New iron-based fluoride cathode material synthesized by non-aqueous ionic liquid for rechargeable sodium ion batteries, Electrochim. Acta 186 (2015) 7–15.
[25] M.L. Jiang, X.Y. Wang, S.Y. Wei, Y.Q. Shen, H. Hu, An ionic-liquid-assisted approach to synthesize a reduced graphene oxide loading iron-based fluoride as a cathode material for sodium-ion batteries, J. Alloys. Compd. 670 (2016) 362–368.
[26] L. Liu, M. Zhou, L.H. Yi, H.P. Guo, J.L. Tan, H.B. Shu, X.K. Yang, Z.H. Yang, X.Y. Wang, Excellent cycle performance of Co-doped $FeF_3$/C nanocomposite cathode material for lithium-ion batteries, J. Mater. Chem. 22 (2012) 17539–17550.
[27] J. Lee, B. Kang, Superior electrochemical performance of N-doped nanocrystalline $FeF_3$/C with a single-step solid-state process, Chem. Commun. 52 (2016) 12100–12103.
[28] Z.H. Yang, Z.J. Zhang, Y.L. Yuan, Y.Q. Huang, X.Y. Wang, X.Y. Chen, S.Y. Wei, A first-principle study of the effect of $OH^-$doping on the elastic constants and electronic structure of HTB-$FeF_3$, RSC Adv. 6 (2016) 75766–75776.
[29] I.D. Johnson, M. Lübke, O.Y. Wu, N.M. Makwana, G.J. Smales, H.U. Islam, R.Y. Dedigama, R.I. Gruar, C.J. Tighe, D.O. Scanlon, F. Cora, D.J.L. Brett, P.R. Shearing, J.A. Darr, Pilot-scale continuous synthesis of a vanadium-doped $LiFePO_4$/C nanocomposite high-rate cathodes for lithium-ion batteries, J. Power Sources 302 (2016) 410–418.
[30] L. Qu, D. Luo, S.H. Fang, Y. Liu, L. Yang, S.i. Hirano, C.C. Yang, Mg-doped $Li_2FeSiO_4$/C as high-performance cathode material for lithium-ion battery, J. Power Sources 307 (2016) 69–76.
[31] X.F. Sun, Y.L. Xu, G.G. Chen, P. Ding, X.Y. Zheng, Titanium doped $LiVPO_4F$ cathode for lithium ion batteries, Solid State Ion. 268 (2014) 236–241.
[32] J.P. Yu, Z.H. Han, X.H. Hu, H. Zhan, Y.H. Zhou, X.J. Liu, The investigation of Ti-modified $LiCoO_2$ materials for lithium ion battery, J. Power Sources 262 (2014) 136–139.
[33] S. Hao, N.Q. Zhao, C.S. Shi, C.N. He, J.J. Li, E.Z. Liu, Enhanced electrochemical properties of $LiCo_{0.5}Ni_{0.5}O_2$ by Ti-doping: a first-principle study, Ceram. Int. 41 (2015) 2294–2300.
[34] M. Wang, M. Yang, L.Q. Ma, X.D. Shen, The high capacity and excellent rate capability of Ti-doped $Li_2MnSiO_4$ as a cathode material for Li-ion batteries, RSC Adv. 5 (2015) 1612–1618.
[35] Z.H. Yang, Z.J. Zhang, Y.L. Yuan, Y.Q. Huang, X.Y. Wang, X.Y. Chen, S.Y. Wei, First-principles study of Ti doping in $FeF_3 \cdot 0.33H_2O$, Curr. Appl. Phys. 16 (2016) 905–913.
[36] N. Yabuuchi, M. Sugano, Y. Yamakawa, I. Nakai, K. Sakamoto, H. Muramatsu, S. Komaba, Effect of heat-treatment process on $FeF_3$nanocomposite electrodes for rechargeable Li batteries, J. Mater. Chem. 21 (2011) 10035–10041.
[37] M. Lengyel, K.Yu Shen, D.M. Lanigan, J.M. Martin, X.F. Zhang, R.L. Axelbaum, Trace level doping of lithium-rich cathode materials, J. Mater. Chem. A 4 (2016) 3538–3545.
[38] P.K. Nayak, J. Grinblat, M. Levi, E. Levi, S. Kim, J.W. Choi, D. Aurbach, Al doping for mitigating the capacity fading and voltage decay of layered Li and Mn-Rich cathodes for Li-Ion batteries, Adv. Energy Mater. 6 (2016) 1502398.
[39] H.F. An, Y. Wang, X.Y. Wang, L.P. Zheng, X.Y. Wang, L.H. Yi, L. Bai, X.Y. Zhang, Polypyrrole/carbon aerogel composite materials for supercapacitor, J. Power Sources 195 (2010) 6964–6969.
[40] Y.G. Wang, H.Q. Li, Y.Y. Xia, Ordered whiskerlike polyaniline grown on the surface of mesoporous carbon and its electrochemical capacitance performance, Adv. Mater. 18 (2006) 2619–2623.
[41] L.F. Jiao, L. Liu, J.L. Sun, L. Yang, Y.H. Zhang, H.T. Yuan, Y.M. Wang, X.D. Zhou, Effect of $AlPO_4$ nanowire coating on the electrochemical properties of $LiV_3O_8$ cathode material, J. Phys. Chem. C 112 (2008) 18249–18254.
[42] F. Wu, J.Z. Chen, R.J. Chen, S.X. Wu, L. Li, S. Chen, T. Zhao, Sulfur/polythiophene with a core/shell structure: synthesis and electrochemical properties of the cathode for rechargeable lithium batteries, J. Phys. Chem. C 115 (2011) 6057–6063.
[43] Y. Bai, X.Z. Zhou, Z. Jia, C. Wu, L.W. Yang, M.Z. Chen, H. Zhao, F. Wu, G. Liu, Understanding the combined effects of microcrystal growth and band gap reduction for $Fe_{(1-x)}Ti_xF_3$ nanocomposites as cathode materials for lithium-ion batteries, Nano Energy 17 (2015) 140–151.
[44] R.S. Rao, V. Pralong, U.V. Varadaraju, Facile synthesis and reversible lithium insertion studies on hydrated iron trifluoride FeF3·0.33H2O, Solid State Sci. 55 (2016) 77–82.
[45] X.P. Xu, S. Chen, M. Shui, L.X. Xu, W.D. Zheng, J. Shu, L.L. Cheng, L. Feng, Y.L. Ren, The investigation of Ti-modified LiCoO2 materials for lithium ion battery, Ionics 20 (2014) 1285–1290.
[46] J. Liu, H. Xia, D.F. Xue, L. Lu, Double-shelled nanocapsules of $V_2O_5$-Based composites as high-performance anode and cathode materials for Li ion batteries, J. Am. Chem. Soc. 131 (2009) 12086–12087.
[47] X. Wang, X.L. Wu, Y.G. Guo, Y.T. Zhong, X.Q. Cao, Y. Ma, J.N. Yao, Synthesis and lithium storage properties of $Co_3O_4$ nanosheet-assembled multishelled hollow spheres, Adv. Funct. Mater. 20 (2010) 1680–1686.